Progress in Neurobiology 222 (2023) 102404

Contents lists available at ScienceDirect

Progress in Neurobiology

journal homepage: www.elsevier.com/locate/pneurobio

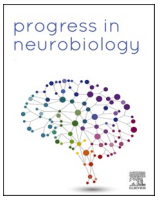

miR-34a regulates silent synapse and synaptic plasticity in mature hippocampus

Xia Min [a,b], Jun-Ying Wang [a,b], Fang-Jiao Zong [a,b], Jing Zhao [a,b], Nan Liu [a,b], Kai-Wen He [a,b,*]

[a] Interdisciplinary Research Center on Biology and Chemistry, Shanghai Institute of Organic Chemistry, Chinese Academy of Sciences, 100 Haike Rd. Shanghai 201210, China
[b] University of Chinese Academy of Sciences, Beijing 100049, China

ARTICLE INFO

Keywords:
miR-34a
Silent synapse
NMDAR
Long-term potentiation
Spatial learning

ABSTRACT

AMPAR-lacking silent synapses are prevailed and essential for synaptic refinement and synaptic plasticity in developing brains. In mature brain, they are sparse but could be induced under several pathological conditions. How they are regulated molecularly is far from clear. miR-34a is a highly conserved and brain-enriched microRNA with age-dependent upregulated expression profile. Its neuronal function in mature brain remains to be revealed. Here by analyzing synaptic properties of the heterozygous miR-34a knock out mice (34a_ht), we have discovered that mature but not juvenile 34a_ht mice have more silent synapses in the hippocampus accompanied with enhanced synaptic NMDAR but not AMPAR function and increased spine density. As a result, 34a_ht mice display enhanced long-term potentiation (LTP) in the Schaffer collateral synapses and better spatial learning and memory. We further found that *Creb1* is a direct target of miR-34a, whose upregulation and activation may mediate the silent synapse increment in 34a_ht mice. Hence, we reveal a novel physiological role of miR-34a in mature brains and provide a molecular mechanism underlying silent synapse regulation.

1. Introduction

Cognitive performance such as learning and memory formation is well known to be developmentally regulated. For example, juvenile learns second language faster than mature adult, which is determined by the age of acquisition rather than duration of learning (Birdsong, 2018). Synaptic plasticity as the major cellular basis for learning and memory formation (Neves et al., 2008; Goto et al., 2021; Kreitzer and Malenka, 2008), its altered mechanisms has been proposed to mediate the developmental switch in cognitive function (Xu et al., 2020; Lee et al., 2005). In juvenile brains, 'unsilencing' the postsynaptically silent synapses, which only express N-methyl-D-aspartate receptors (NMDARs) but not α-amino-3-hydroxy-5-methyl-4-isoxazolepropionic acid receptor (AMPARs) in postsynaptic compartment (Isaac et al., 1995; Liao et al., 1995), efficiently mediates synaptic potentiation and contributes to the heightened plasticity during critical period (Xu et al., 2020; Vincent-Lamarre et al., 2018). While silent synapses are abundant during early development, they disappear or become rare in mature adult brains (Xu et al., 2020; Kerchner and Nicoll, 2008). The switching into silent synapse-independent plasticity may underlie the cognitive changes in adult. Furthermore, silent synapses could be induced in mature brains under physiological condition such as learning (Wang et al., 2019). They are also tightly associated with many neuropathological conditions such as addiction (Hanse et al., 2013; Koya et al., 2012; Wright et al., 2020), seizure (Sun et al., 2018), pain (Wang et al., 2021) and Alzheimer's diseases (Bie, 2018), which is found to mediate abnormal synaptic transmission and synaptic plasticity. How silent synapses are regulated in mature brains and what molecules are critically involved remain largely unknown.

MicroRNAs (miRNAs) are small non-coding RNAs critical for post-transcriptional regulation by binding to the 3′ untranslated region (3′UTR) of their target mRNAs (Bartel, 2009; Gebert and MacRae, 2019). Hundreds of miRNAs are identified in the central nervous system (CNS) and many of them have important neural function (Nowakowski et al., 2018; Kosik, 2006; Abe and Bonini, 2013; Schratt, 2009). Among these miRNAs, we are particularly interested in miR-34a, which is highly

Abbreviations: NMDAR, N-methyl-D-aspartate receptor; AMPAR, α-amino-3-hydroxy-5-methyl-4-isoxazolepropionic acid receptor; LTP, long-term potentiation; LTD, long-term depression.

* Corresponding author at: Interdisciplinary Research Center on Biology and Chemistry, Shanghai Institute of Organic Chemistry, Chinese Academy of Sciences, 100 Haike Rd. Shanghai 201210, China.
E-mail address: kwhe@sioc.ac.cn (K.-W. He).

https://doi.org/10.1016/j.pneurobio.2023.102404
Received 18 October 2022; Received in revised form 26 December 2022; Accepted 11 January 2023
Available online 13 January 2023

conserved across species (Chang et al., 2007), selectively enriched in brain tissue (Bommer et al., 2007), and upregulated with brain maturation and aging (Jauhari et al., 2018). Several studies reported that miR-34a modulates cell differentiation (Aranha et al., 2011) and synaptogenesis (Agostini et al., 2011) during early neural development. On the other hand, abnormal elevation in miR-34a is observed in aged and neurodegenerative brains (Kou et al., 2017, 2016; Chen et al., 2019), which is associated with impaired synaptic transmission and/or plasticity (Sarkar et al., 2016; Xu et al., 2018; Hu et al., 2019; Cogswell et al., 2008). These findings suggest that miR-34a plays essential role in synaptic regulation. While its expression plateaus and remains stable throughout adulthood (Jauhari et al., 2018), its synaptic function in mature brain is far from clear.

In the current study, we examined the synaptic role of miR-34a in mature adult hippocampus by utilizing the heterozygous miR-34a knockout mice (34a_ht). We surprisingly found that reducing miR-34a promotes synaptic NMDARs function and increases silent synapse density in CA1 pyramidal neurons, which leads to enhanced long-term potentiation (LTP) of the Schaffer collateral synapses and better spatial learning and memory of the 34a_ht mice. We further identified that the transcription factor *Creb-1* as a direct target of miR-34a, whose upregulation correlates with the silent synapse phenotype in mature 34a_ht mice. Therefore, our study demonstrates an important role of miR-34a in regulating synaptic plasticity by targeting silent synapse formation in mature brain.

2. Results

2.1. Selectively enhanced NMDAR-mediated synaptic transmission of hippocampal Schaffer collateral synapses in 34a_ht mature adult mice

Heterozygous miR-34a knockout mice (34a_ht) were employed in current study. miR-34a expression was down-regulated by 50–60% in hippocampi of 34a_ht mice without changing levels of the other two miR-34 family members, miR-34b and c (Fig. 1A). miR-34a homozygotes knockout mice (34a_hm) were rarely obtained (Fig S1A), which is likely due to its important neurodevelopmental role reported previously (Aranha et al., 2011; Chang et al., 2011; Mollinari et al., 2015; Morgado et al., 2015). We first compared the hippocampal transcriptomes between mature (6–9-month-old) 34a_ht and their WT littermates (Fig S1B) and synapse-related terms were enriched by performing Gene Ontology (GO) analysis (Zhou et al., 2019) (Fig S1C), supporting our hypothesis that synaptic regulation is one of the most important brain functions of miR-34a in mature brains.

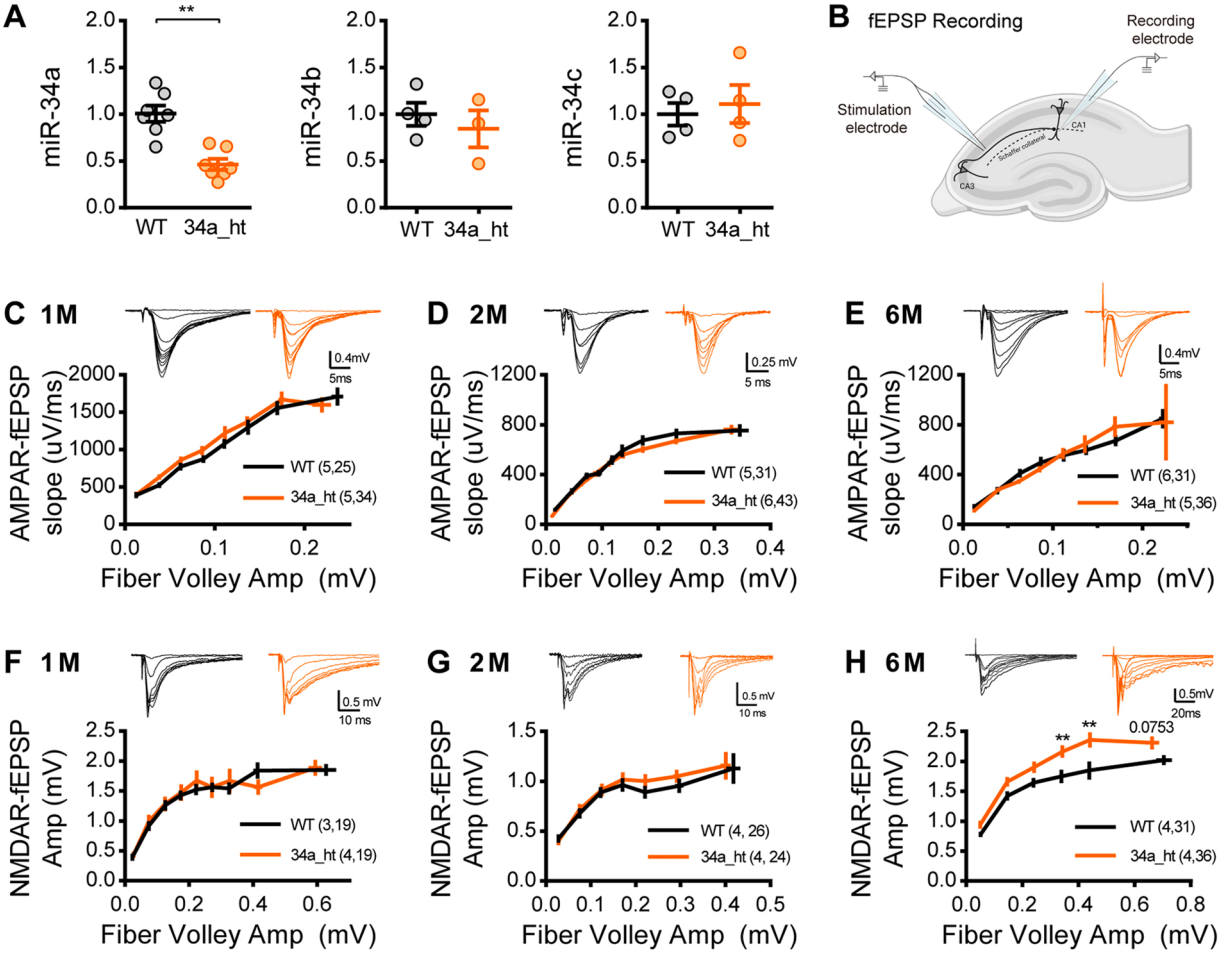

Fig. 1. Selectively enhanced NMDAR-mediated synaptic transmission of hippocampal Schaffer collateral synapses in 34a_ht mature adult mice. (A) Relative expression of miR-34a (Left panel, WT = 1.000 ± 0.08547, 34a_ht = 0.4605 ± 0.05774; n = 7; P = 0.0023), miR-34b (Middle panel, WT = 1.000 ± 0.1235, 34a_ht = 0.8442 ± 0.1996; n = 4; p = 0.5714), and miR-34c (Right panel, WT = 1.000 ± 0.1212, 34a_ht = 1.111 ± 0.2028; n = 4; p > 0.9999) in hippocampus of mature adult mice (Mann Whitney test). (B) Schematic diagram showing fEPSP recording at the Schaffer collateral pathway from acute hippocampal slices. (C-E) Comparison of AMPAR-dependent basal synaptic transmission by fEPSP recording between 34a_ht and their wildtype littermates at different ages. 1-month-old (C), 2-month-old (D) and 6-month-old (E). (F-H) Comparison of NMDAR-dependent basal synaptic transmission by fEPSP recording between 34a_ht and their wildtype littermates at different ages. 1-month-old (F), 2-month-old (G) and 6-month-old (H, F (1, 334) = 40.67, P < 0.0001, Two-way ANOVA with Sidak's multiple comparisons test). For panels C-H, sample size is indicated as (mice, slices). (* P < 0.05; ** P < 0.01).

We next examined synaptic properties of Schaffer collateral CA1 synapses by extracellular field excitatory postsynaptic potential (fEPSP) recording (Fig. 1B). Presynaptic function was measured by paired-pulse ratio (Fig S1D), while postsynaptic properties were interrogated by comparing both AMPA receptor (AMPAR)- and NMDAR receptor (NMDAR)-mediated basal synaptic transmission (Fig. 1C-H). CA1 synapses in both 1- and 2-month-old juvenile 34a_ht mice remained generally normal compared to the age-matched wildtype littermates (Figs. 1C-D, 1F-G, Fig S1D left and middle panels), indicating that reducing miR-34a does not affect early neural development and synaptic function at young age. Several previous studies reported age-dependent increase in brain expression of miR-34a (Jauhari et al., 2018; Kou et al.,

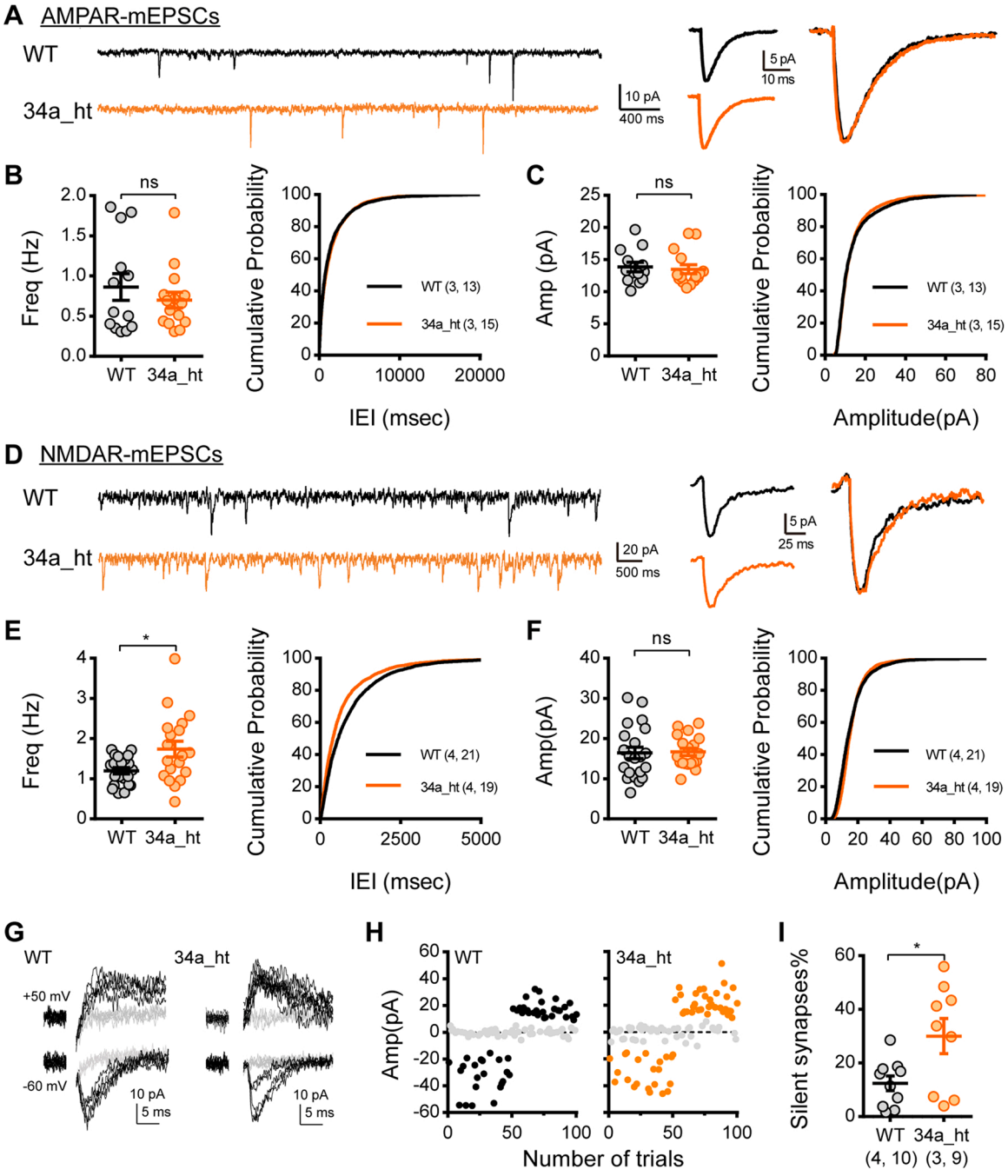

Fig. 2. More silent synapses in CA1 neurons from 34a_ht mature adult mice. (A) Example traces of AMPAR-mEPSC recordings (Left) and average mEPSC waveforms (Right). (B-C) AMPAR-mEPSC comparison between 34a_ht and WT mice. Left panels in B & C, mean frequency (B, WT = 0.8628 ± 0.1649 Hz; 34a_ht = 0.7011 ± 0.09856 Hz; P = 0.9174) and amplitude (C, WT = 13.86 ± 0.7354 pA; 34a_ht = 13.51 ± 0.7022 pA; P = 0.4905). Right panels in B & C, cumulative probability histograms of the inter-event intervals (B, K-S test, P = 0.0536) and mEPSC amplitude (K-S test, P = 0.0980). (D) Example traces of NMDAR-mEPSC recordings (Left) and average mEPSC waveforms (Right). (E-F) NMDAR-mEPSC comparison between 34a_ht and WT mice. Left panels in E & F, mean frequency (E, WT = 1.199 ± 0.07652; 34a_ht = 1.737 ± 0.1961; P = 0.0290) and amplitude (F, WT = 16.45 ± 1.443pA; 34a_ht = 16.69 ± 0.9042pA; P = 0.6248). Right panels in E & F, cumulative probability histogram of the inter-event intervals (E, K-S test, P < 0.0001) and mEPSC amplitude (K-S test, P < 0.0001). (G-I) Silent synapse recordings by minimal stimulations. (G) Example traces (successful or failed) elicited by minimal stimulations at + 50 mV (top) and − 60 mV (bottom) from WT and 34a_ht mice. (H) Trial plots of EPSCs elicited by minimal stimulations at + 50 and − 60 mV from WT and 34a_ht mice. (I) Percentage of silent synapses in CA1 neurons of WT and 34a_ht mice (WT = 12.42 ± 2.756%; 34a_ht: 30.05 ± 6.556%; P = 0.0434). Sample size is indicated as (mice, cells). Mann Whitney test. * P < 0.05.

2017, 2016; Chen et al., 2019; Liu et al., 2012; Huang et al., 2017). Therefore, we wondered whether CA1 synapses in fully mature brain will be affected. At the age of 6–9 months, presynaptic function (Fig S1D right panel) as well as AMPAR-dependent basal synaptic transmission were still comparable between WT and 34a_ht mice (Fig. 1E). Surprisingly, we found that the input-output curve of the isolated NMDAR responses was significantly up-shifted in 34a_ht mice (Fig. 1H), indicating an enhanced NMDAR-mediated synaptic transmission. In summary, our results suggest that miR-34a selectively regulates postsynaptic NMDAR but not AMPAR function and presynaptic properties in mature but not juvenile hippocampus.

2.2. CA1 pyramidal neurons in mature 34a_ht mice have increased silent synapses

Two possibilities could explain the enhanced NMDAR- but not AMPAR-mediated basal synaptic transmission. One is by increasing synaptic NMDARs expression (Carroll and Zukin, 2002; Lau and Zukin, 2007) or by changing NMDAR subunit composition (Kohr, 2006; Paoletti et al., 2013). The other is by having more AMPAR-lacking postsynaptically silent synapses (Isaac et al., 1995; Liao et al., 1995; Kerchner and Nicoll, 2008). We next sought to distinguish between these two possibilities by first analyzing AMPAR- and NMDAR-conducted synaptic currents. Pharmacologically isolated AMPAR- and NMDAR-mediated miniature excitatory postsynaptic currents (AMPAR-mEPSCs, NMDAR-mEPSCs) of CA1 pyramidal neurons were recorded and compared between mature 34a_ht and their wildtype littermates (Fig. 2A and D, see methods). Neither the amplitude (Fig. 2C) nor the frequency (Fig. 2B) of AMPAR-mEPSCs was different between groups, further supporting that miR-34a does not affect postsynaptic AMPAR function and presynaptic release. In turns of NMDAR-mEPSCs, the cumulative distribution of the current amplitude was differed (Fig. 2F right panel) but the mean current amplitude was unchanged (Fig. 2F left panel) with similar current decay kinetic (Fig S2B right panel). These results suggest heterogeneous alteration but on average normal postsynaptic NMDAR density and subunit composition in 34a_ht mice. Interestingly, frequency of the NMDAR-mEPSCs was significantly higher in 34a_ht mice (Fig. 2E). Change in mEPSC frequency is usually attributed to altered presynaptic function or synaptic numbers (Redman, 1990; Korn and Faber, 1991). Since presynaptic property is maintained, the higher NMDAR-mEPSC frequency indicates that 34a_ht mice have more NMDAR-containing synapses.

The unaltered AMPAR- but elevated NMDAR-mEPSCs frequency suggest that mature 34a_ht mice may have increased number of AMPAR-lacking silent synapses in hippocampal CA1 pyramidal neurons. To directly compare the silent synapse density between 34a_ht and wildtype mice, we performed minimal stimulation assay (Isaac et al., 1995; Liao et al., 1995). Stimulation intensity was adjusted to achieve interleaved failure of AMPAR responses when CA1 pyramidal neuron was voltage clamped at − 60 mV. Percentage of silent synapse was then calculated by comparing the failure rates of NMDAR and AMPAR responses (See Methods). In lines with the mEPSC alterations, the 34_ht mice had reduced NMDAR failure rate (Fig. 2G, H & S2C) and significantly higher percentage of silent synapses (Fig. 2I). Thus, these electrophysiological evidences unveil that reducing miR-34a in mature brain indeed promotes silent synapse generation in the hippocampus.

2.3. Structural and biochemical evidences for increased silent synapses in mature 34a_ht mice

Our functional analyses suggest more silent synapses in mature 34a_ht mice, which is probably due to the addition of NMDAR-only synapses rather than removing AMPAR from pre-existing functional synapses. To further verify this unexpected phenomenon, we quantified the spine density of CA1 pyramidal neurons in both 34a_ht and WT mice by delivering GFP-carried lentivirus into dorsal CA1 (Fig. 3A, see

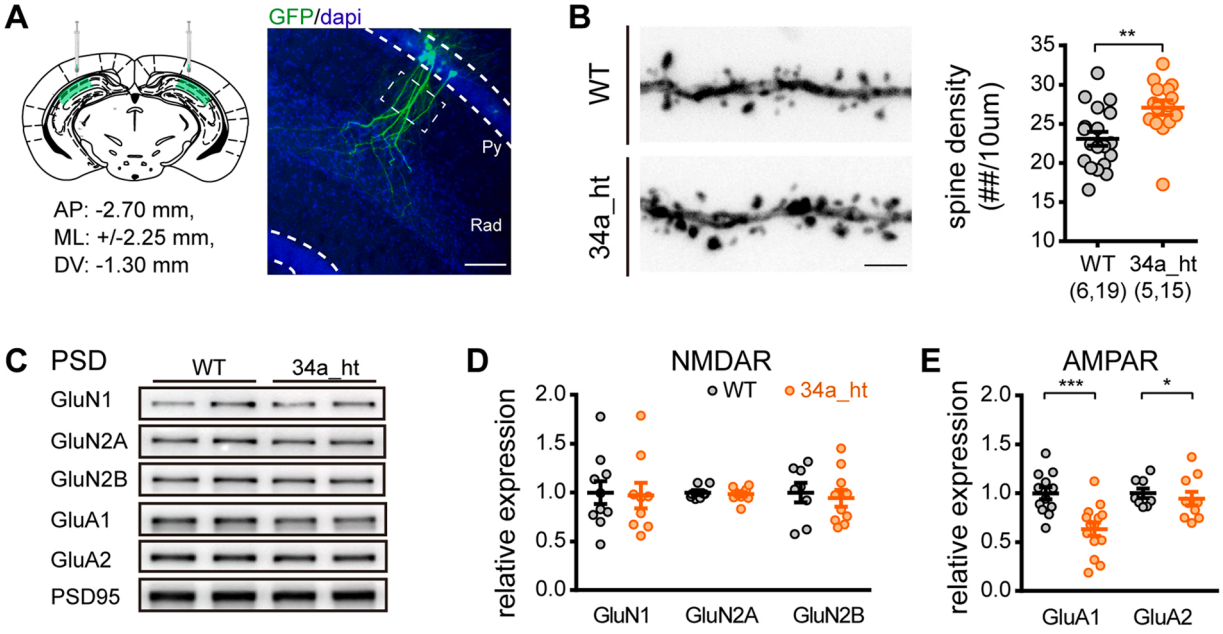

Fig. 3. Increased dendrite spine density and reduced synaptic AMPAR expression in the hippocampus of adult 34a_ht mice. (A) Schematic of intrahippocampal injection of Tet-off GFP lentivirus (left panel) and representative image of sparse labeled CA1 pyramidal neurons (right panel). Scale bars, 100 μm. (B) Quantification of CA1 pyramidal neuron basal dendritic spine density (WT = 23.08 ± 0.8976/10 μm; 34a_ht: 27.06 ± 0.9221/10 μm; P = 0.0035). Left: representative images of dendritic segments of GFP-labeled CA1 pyramidal neurons from WT and 34a_ht mice. Scale bar, 10 μm. (C-E) Examination of synaptic protein expression levels. (C) Sample blots showing protein expression in isolated fraction of postsynaptic density (PSD). (D) Quantification of synaptic NMDAR subunit GluN1, GluN2A, and GluN2B in WT and 34a_ht mice (GluN1: WT = 1.000 ± 0.1185, 34a_ht = 0.9697 ± 0.1307, P = 0.7019; GluN2A: WT = 1.000 ± 0.02411, 34a_ht = 0.9833 ± 0.02186, P > 0.9999; GluN2B: WT = 1.000 ± 0.09917, 34a_ht = 0.9428 ± 0.08659, P = 0.7493; n = 8 & 10 for WT & 34a_ht). (E) Quantification of synaptic AMPAR subunit GluA1 and GluA2 in WT and 34a_ht mice (GluA1: WT = 1.000 ± 0.06198, 34a_ht = 0.6319 ± 0.06848, P = 0.0005; GluA2: WT = 1.000 ± 0.03973, 34a_ht = 0.8901 ± 0.05521, P = 0.0269; n = 12 & 14 for WT & 34a_ht). Mann Whitney test, * P < 0.05; * * P < 0.01; * ** P < 0.001.

method). Only spines on the secondary and/or tertiary apical dendrites were imaged and analyzed. In agreement with the functional alteration, a significant increase in spine density was found in 34a_ht mice compared to their wildtype controls (Fig. 3B). This result provides structural evidence supporting that reducing miR-34a in mature brain promotes synaptic NMDAR function via generating new silent synapses.

Silent synapses only express NMDARs but not AMPARs in postsynaptic compartment. More silent synapses should be associated with reduced mean postsynaptic AMPARs. We thus examined the synaptic expression of NMDARs and AMPARs by enriching postsynaptic density (PSD) from hippocampal tissue (Fig S3D, see Methods). Synaptic levels of NMDARs and AMPARs were normalized to that of PSD95, the main excitatory postsynaptic scaffolding protein whose synaptic density remained unchanged (Fig S3F). We found no change in NMDAR

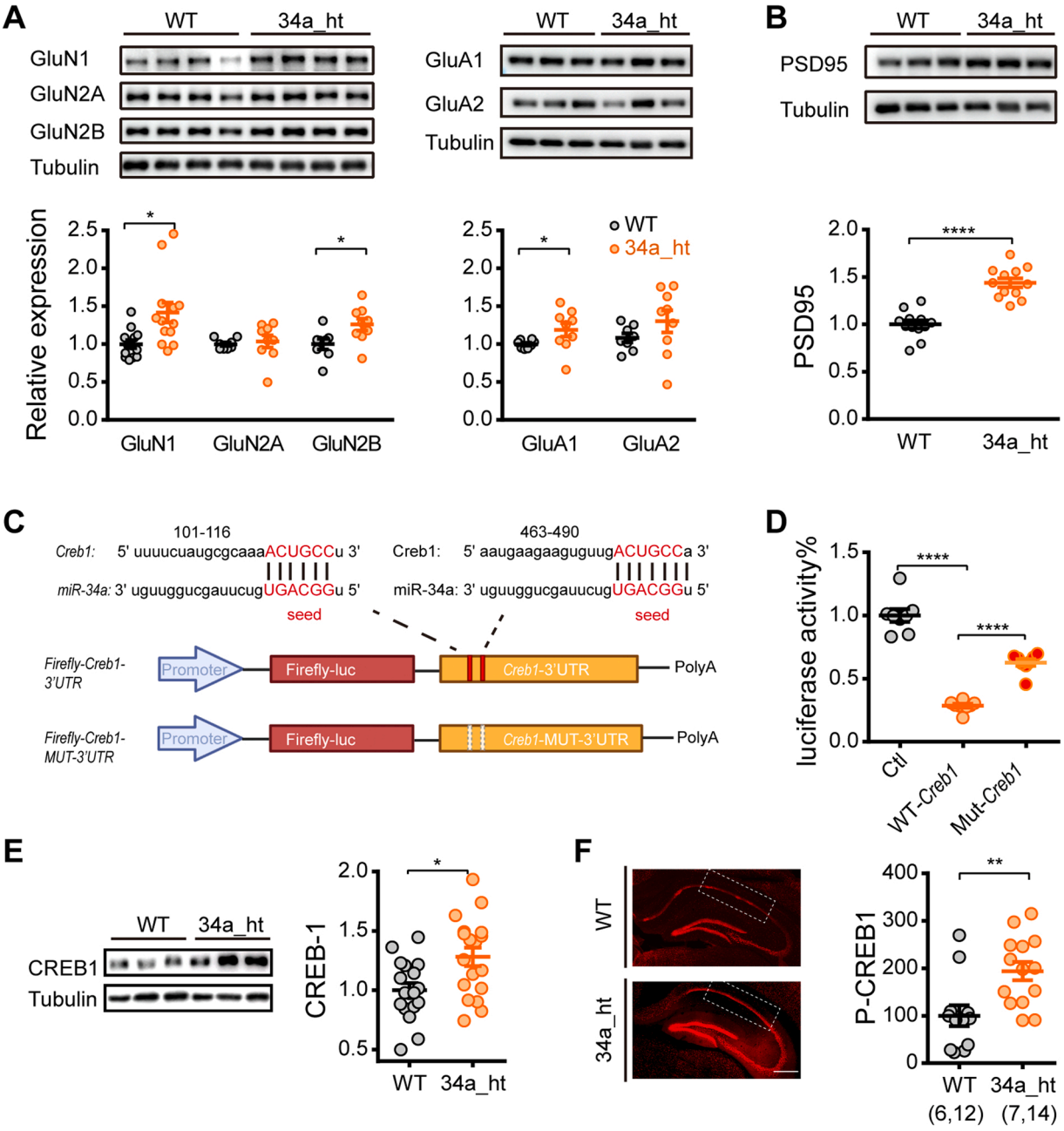

Fig. 4. *Creb1* is a direct target of miR-34a. (A-C) Sample blots (top panels) and quantification of total protein levels of hippocampal NMDARs (A, GluN1: 1.000 ± 0.05156 vs. 1.419 ± 0.1312, P = 0.0015; GluN2A: 1.000 ± 0.02460 vs. 1.036 ± 0.08151, P = 0.4688; GluN2B: 1.000 ± 0.06821 vs. 1.259 ± 0.07934, P = 0.0152; n = 8 & 9 for WT & 34a_ht), AMPARs (B, GluA1:1.000 ± 0.01913 vs. 1.189 ± 0.08926, P = 0.0359; GluA2: 1.000 ± 0.05417 vs. 1.203 ± 0.1345, P = 0.1373; n = 8 & 9 for WT & 34a_ht), and PSD95 (C, WT: 1.000 ± 0.04106; 34a_ht: 1.438 ± 0.04710, P < 0.0001; n = 12 & 12 for WT & 34a_ht) in WT and 34a_ht mice. (C) Schematic diagram showing the constructs of firefly-luciferase-*Creb1*-3′UTR (WT-*Creb1*) and firefly-luciferase-*Creb1*-MUT-3′UTR (Mut-*Creb1*). HEK293T cells were transfected with WT-*Creb1* only (Ctl) or co-transfected with WT-*Creb1* and miR-34a (WT-*Creb1*), or co-transfected with Mut-*Creb1* and miR-34a (Mut-*Creb1*). (D) Comparison of luciferase activities among control, WT-*Creb1* and Mut-*Creb1* (Ctl = 1.000 ± 0.05005; WT-*Creb1* = 0.2869 ± 0.01515; Mut-*Creb1* = 0.6277 ± 0.02668; One-way ANOVA F (2,21) = 1.478, P < 0.0001). (E) Normalized total CREB1 protein levels in hippocampus of wildtype and 34a_ht mice (WT = 1.000 ± 0.05838; 34a_ht = 1.281 ± 0.07858, P = 0.0106). Sample blots on the right. (F) Immunochemical staining of phosphorylated CREB1 Ser-133 (P-CREB) in the hippocampus of wildtype and 34a_ht mice. Left panel, representative images. Right panel, normalized P-CREB signal intensity in CA1 region (WT = 100.0 ± 22.15; 34a_ht = 194.2 ± 19.53, P = 0.0077). Sample size is indicated as (mice, cells) in E & F. Mann Whitney test, * P < 0.05; * * P < 0.01; * ** * P < 0.0001.

subunits, including GluN1, GluN2A and GluN2B, in 34a_ht mice (Fig. 3C-D), which is consistent with the unaltered NMDAR-mEPSC amplitude and kinetic. In contrast, synaptic level of GluA1 and GluA2, which are the main subunits of AMPARs, were significantly reduced in 34a_ht mice (Fig. 3C & E). Thus, the synaptic profiles of NMDARs and AMPARs again support more silent synapses in mature 34a_ht mice.

2.4. miR-34a regulates silent synapses by directly targeting CREB1

We now have provided functional, structural, and biochemical evidences of more silent synapses in hippocampus of mature 34a_ht mice. Next, we wondered what downstream mechanism might mediate such regulation following miR-34a reduction. Protein levels of NMDARs and synaptic scaffolding proteins such as PSD95 are implicated in silent synapse regulation (Hanse et al., 2013; Nakayama et al., 2005; Huang et al., 2015; Yusifov et al., 2021; Shukla et al., 2017). We did find moderate but significant increase in NMDARs subunits GluN1 and GluN2B, AMPAR subunit GluA1 and PSD95 in total hippocampal homogenate (Fig. 4A & B). Among these upregulated proteins, only GluN2B is the direct target of miR-34a (Sarkar et al., 2019). The other three did not have the binding sequence for miR-34a, their increase is likely via indirect signaling pathway. cAMP response element-binding protein 1 (CREB1) as a classical transcription factor is important for synaptogenesis and synaptic plasticity (Lee et al., 2007; Lonze and Ginty, 2002; Lisman et al., 2018; Aguado et al., 2009), whose activation has been shown to elevate transcription of *Grin1*, *Grin2B*, and *Dlg4* (Telese et al., 2015). Furthermore, overexpression of activated form of CREB1 has been shown to promote silent synapse formation (Marie et al., 2005; Brown et al., 2011). Intriguingly, *Creb1* is predicted to be direct target of miR-34a by sequence analysis (Paraskevopoulou et al., 2013; Reczko et al., 2012) (Fig S4A), suggesting that reducing miR-34a may increase the expression of synaptic proteins via directly upregulating CREB1 level.

To test whether *Creb1* is direct target of miR-34a, firefly luciferase assay was designed and performed. *Creb1* is predicted to have two seeding regions for miR-34a-5p in its 3′ UTRs (Fig. 4C). We therefore generated firefly luciferase reporter by fusing the coding region of luciferase to the 3′ UTR of *Creb1* (*Creb1-Luc*, See methods). Co-transfection of miR-34a caused around 70% reduction in the expression of *Creb1-Luc*, which could be largely prevented by mutating both seeding regions (Fig. 4D). These results indicate that miR-34a can indeed directly regulate *Creb1* translation by binding to its seeding regions. In line with the in vitro result, 34a_ht mice did have significantly upregulated protein level of CREB1 in the hippocampus (Fig. 4E), further validating the direct targeting of *Creb1* by miR-34a. CREB1 activation requires phosphorylation of the serine 133 (S133) site (Gonzalez and Montminy, 1989; Naqvi et al., 2014). We observed almost two times increase in signal intensity of S133-phosphorated CREB1 in CA1 region of 34a_ht mice compared to their wildtype littermates (Fig. 4F), suggesting that CREB1 is more strongly activated. All these findings together suggest that miR-34a targets *Creb1* directly, which may then control the expression of critical synaptic proteins and might contribute to the generation of silent synapses in mature hippocampus.

2.5. Mature 34a_ht mice have enhanced hippocampal long-term potentiation and better spatial learning

'Unsilencing' the silent synapses by recruiting AMPARs into postsynaptic membrane is one important mechanism underlying long-term potentiation (LTP) (Vincent-Lamarre et al., 2018; Hanse et al., 2013) especially during early development when silent synapses are the most abundant (Ashby and Isaac, 2011; Busetto et al., 2008). In mature brain, silent synapses are still present but at very low level and thus are not considered significant for LTP (Sametsky et al., 2010). Our current findings show that reducing miR-34a increases silent synapse density and postsynaptic NMDAR function in mature hippocampus, we therefore speculated that LTP induction and expression might be facilitated in 34a_ht mice. We therefore quantified and compared synaptic plasticity in Schaffer collateral CA1 synapses by fEPSP recording. LTP was induced by delivering four trains of theta burst stimulation (TBS) after establishing stable baseline (see Method). As expected, 34a_ht mice had significantly larger LTP than their wildtype littermates (Fig. 5A & B), suggesting an enhanced LTP expression. Consistent with the increased postsynaptic NMDAR conductance, response summation during the first 3 theta bursts of each train stimulation was larger in 34a_ht mice (Fig S5A), indicative of more efficient LTP induction. No change in pair-pulse ratio before or after the induction of LTP for either genotype (Fig S5B), suggesting presynaptic mechanism is unlikely involved. Therefore, we found mature 34a_ht mice express greater LTP in Schaffer collateral synapses, which is in line with their increase in silent synapses. In contrast, NMDAR-dependent long-term depression (LTD) induced by prolong pair-pulsed 1 Hz stimulation (Collingridge et al., 2010) was not affected in 34a_ht mice (Fig. 5 C & D). This finding indicates that NMDARs in functional synapses remain unaltered, which is in agreement with all other results. Similar to the age-dependent change in NMDAR-mediated basal synaptic transmission, enhancement in LTP was also limited to mature but absent in juvenile hippocampus (Fig S5C-F).

Synaptic plasticity is considered as cellular mechanism for learning and memory (Martin et al., 2000). Since mature 34a_ht mice have enhanced LTP, we wondered whether their learning and/or memory performance will be different. We first examined the short-term memory by running Y-maze test (Fig S6A). The mean alternations were not distinct between the two groups (Fig S6B), suggesting normal short-term memory in mature 34a_ht mice. Since Y-maze requires both the hippocampus and the prefrontal cortex (Kraeuter et al., 2019), we next sought to test their hippocampus-dependent spatial learning and memory using novel object location task (NOL, Fig. 6A, See Methods). Wildtype littermates hardly memorized the object locations with brief training. In contrast, 34a_ht mice showed significantly better discrimination 1 h post training (Fig. 6B), suggesting an improved spatial learning and memory. 34a_ht mice' enhanced hippocampal function was further validated using the Barnes maze Test (Fig. 6C, See Methods). Consistently, 34a_ht mice showed faster learning than their wildtype littermates reflected by steeper learning curves (Fig. 6D & Fig S6D-F). They achieved their best performance by the 4th day of training while the wildtype littermates needed another 2 days of training (Fig. 6D & Fig S6G-I). The faster learning was not due to difference in general locomotor ability (Fig S6C & S6J). In the probe test trial, 34a_ht mice showed a trend of better memory (Fig. 6E). Hence, reducing miR-34a level in mature hippocampus promotes hippocampal-dependent spatial learning and memory.

3. Discussion

miR-34a is highly conserved across species and enriched in the brain. Increasing evidences suggest that miR-34a has important neuronal function during early neural development. Its role in mature and aged brain has attracted more and more attention due to its age-dependent and neurodegeneration-associated increase in expression. Here we found that miR-34a selectively regulates synaptic NMDAR function and synaptic plasticity in fully mature but not juvenile hippocampus by promoting silent synapse formation. We further discover that transcription factor *Creb1* is a direct target of miR-34a, whose elevation and activation correlate with the formation of silent synapses in mature 34a_ht mice. To this end, our findings unveil a novel physiological function of miR-34a in mature adult brain (Fig. 7).

Silent synapses are present in high abundance during early postnatal development but only scarcely found in adult brain. Most of them are pruned during brain maturation, some are 'unsilenced' in an experience-dependent manner to stabilize synapses and circuits (Hanse et al., 2013). By providing physiological, structural, and biochemical evidences, our findings strongly support a silent synapse-specific synaptogenic role of

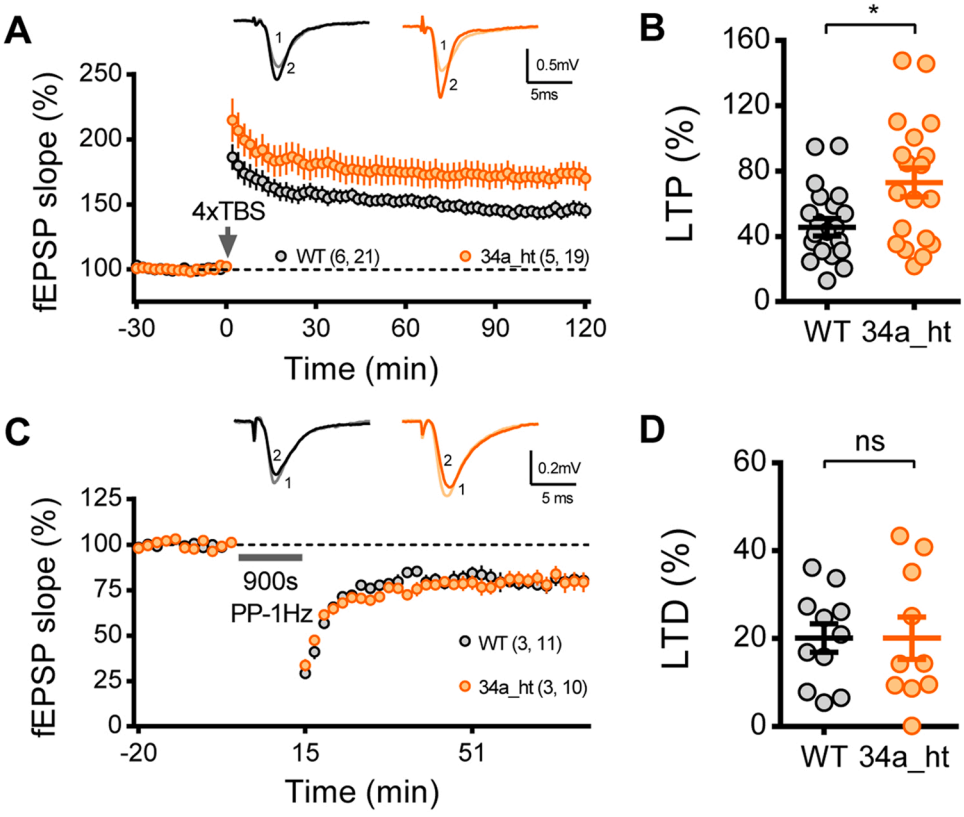

Fig. 5. Enhanced hippocampal long-term potentiation in mature 34a_ht mice. (A) Summary of LTP time course of WT and 34a_ht mice. Top, representative average fEPSP traces pre- (−4 to 0 min, gray and light orange) and post-TBS (116–120 min, black and orange). (B) Quantification of LTP magnitude (average of 111–120 min) (WT = 45.52 ± 5.376%; 34a_ht = 73.07 ± 8.831%; P = 0.0312). (C) Summary of LTD time course of WT and 34a_ht mice. Top, representative average fEPSP traces pre- (−4 to 0 min, gray and light orange) and post-PP-1 Hz (71–75 min, black and orange). (D) Quantification of LTD magnitude (average of 66–75 min) (WT = 20.16 ± 3.214%; 34a_ht = 20.10 ± 4.776%; P = 0.9515). Sample size is indicated as (mice, cells). Mann Whitney test, * $P < 0.05$.

miR-34a in adult hippocampus, which is supported by previous study showing that pre-miR-34a overexpression in cultured hippocampal neurons significantly reduces filopodia (Agostini et al., 2011), an immature form of synapses that is commonly considered silent (Watson et al., 2016). On the other hand, conditional miR-34a overexpression in adult mice caused short- and long-term spatial memory deficit (Sarkar et al., 2019). Since pyramidal neurons in mature and aged brains still possess few silent synapses (Sametsky et al., 2010), overexpression of miR-34a in adult might impair hippocampal function partially by targeting this population of synapses.

Interestingly, we found that this neuronal function of miR-34a is both age- and brain region-specific. Neither postsynaptic NMDAR function in young hippocampus, nor spine density in adult visual cortex of 34a_ht mice is changed, suggesting that the miR-34a-mediated regulation of silent synapse formation is both temporally and spatially tuned. This might be related to the developmental profile of silent synapses as well as the expression pattern of miR-34a. miR-34a is previously shown to be developmentally upregulated (Jauhari et al., 2018; Kou et al., 2017; Liu et al., 2012; Huang et al., 2017). In mature brain, we further found that it has very distinct expression patterns across different brain regions (Fig S3A). It is possible that the level of miR-34a might be one important determinant of silent synapse formation. Other regulatory mechanisms for silent synapse formation may also exist at different developmental stages and brain regions. For example, overexpression of active form of CREB1 is reported to be sufficient to trigger silent synapse formation (Marie et al., 2005; Brown et al., 2011). In adult 34a_ht mice, increased CREB1 correlates with more silent synapses in the hippocampus. While miR-34a can directly modulate the protein level of CREB1, its activation measured by serine-133 phosphorylation is differently regulated in the hippocampus and visual cortex of the 34a_ht mice (Fig. 4 F & Fig S4C), suggesting that additional signal is required for CREB1-mediated silent synapse formation. In addition to pyramidal neurons, other types of neurons such as GABAergic neurons in the hippocampus (Riebe et al., 2009) and Purkinje cells in the cerebellum (Dean et al., 2010) are reported to maintain large amount of silent synapse even in mature adult brain. Whether miR-34a similarly regulate silent synapses in these cell types will be of interest for future study.

Conversion of silent into functional synapses by recruiting synaptic AMPARs is considered one major cellular mechanism underlying synaptic strengthening during critical period (Xu et al., 2020). Promoting silent synapse formation might therefore help rejuvenate the adult plasticity. Indeed, we found that adult 34a_ht mice display enhanced Schaffer collateral LTP and better hippocampus-dependent spatial learning and memory along with increased silent synapses, suggesting rejuvenating potential of reducing miR-34a expression in fully mature hippocampus. This is supported by one study reporting that miR-34a knockout in Alzheimer's disease model mice APP/PS1 improved the hippocampus-mediated cognitive function (Jian et al., 2017). Beside the potential benefit of having more silent synapses in the hippocampus, the aberrant appearance of silent synapses in other brain regions is also implicated in several neuropathological conditions, such as addiction (Brown et al., 2011; Lee et al., 2013; Beroun et al., 2018) and neuropathic pain (Wang et al., 2021). What molecular signals may trigger silent synapse generation under these conditions remain largely unclear. Whether miR-34a is involved will be intriguing to examine.

4. Materials and methods

4.1. Animals

All experimental procedures were approved by the Institutional Animal Care and Use Committees at the Interdisciplinary Research Center on Biology and Chemistry, Chinese Academy of Science. miR-34a heterozygotes (34a_ht, GemPharmatech Co., Ltd) and their wildtype (WT, genetic background: C57BL/6 J) littermates of 1- and 2-month-old or 6–9-month-old (mature adult) were used. Both juvenile female and male mice were used but only male adult mice were used in this study. All mice were group housed in standard cages with regular 12 h:12 h

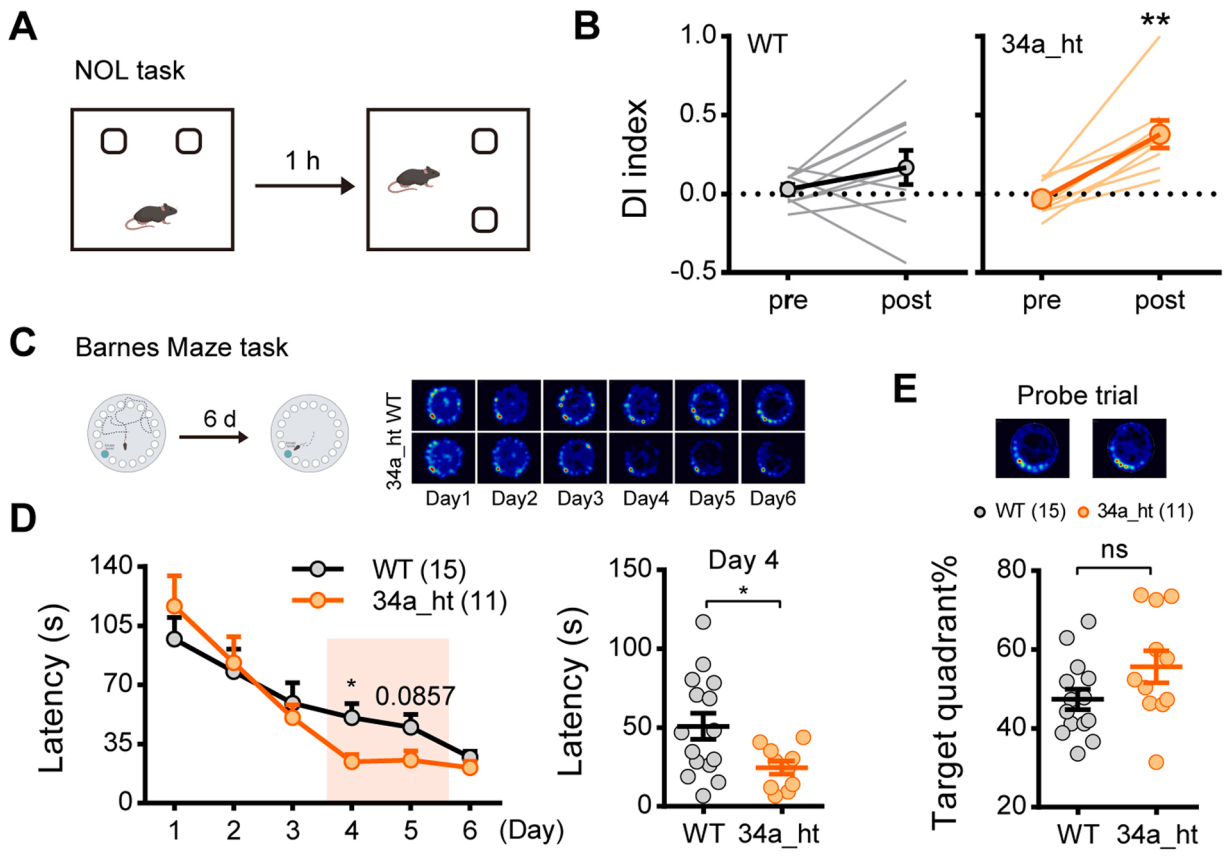

Fig. 6. Mature 34a_ht mice have better spatial learning ability. (A-I) Analysis of spatial learning and memory with Novel location recognition task and Barnes maze task. (A) Schematic of Novel location recognition task. (B) Discrimination index in the OLM task before and after familiarizing object location (WT-pre = 0.029 ± 0.099; WT-post = 0.168 ± 0.344; P = 0.2324; 34a_ht-pre = −0.032 ± 0.103; 34a_ht-post = 0.380 ± 0.263; P = 0.0039). (C) Schematic of Barnes maze (top) and representative heatmaps of escape traces during learning. (D) Mean latency to escape for WT and 34a_ht mice during training. Left, learning curves showing the mean latency to escape. Right, quantification of the mean level of two trials on the 4th day of training (Left, WT = 50.73 ± 8.254 s; 34a_ht = 24.61 ± 4.238 s; P = 0.0408; Right, WT = 44.89 ± 7.683 s; 34a_ht = 25.45 ± 5.610 s; P = 0.0857). (E) Top: Representative heatmaps of escape traces in probe test. Bottom: Quantification of duration in target quadrant for both WT and 34a_ht mice (WT = 47.36 ± 2.611 s; 34a_ht = 55.63 ± 4.085 s; P = 0.1102). Statistic: Wilcoxon matched-pairs signed rank test; Mann Whitney test, * P < 0.05, * * P < 0.01.

light/dark cycle and ad libitum access to food and water.

4.2. Electrophysiology

4.2.1. Acute brain slices preparation

For fEPSP recording, acute 400 μm-thick transverse hippocampal slices were prepared as described previously (He et al., 2015). Briefly, mice were anesthetized with isoflurane vapor and whole brain was quickly removed. Hippocampi were isolated and slices were cut using a vibratome (Leica). Tissue was maintained in ice-cold dissection buffer (212.7 mM sucrose, 5 mM KCl, 1.25 mM NaH_2PO_4, 10 mM $MgCl_2$, 0.5 mM $CaCl_2$, 26 mM $NaHCO_3$, and 10 mM dextrose, bubbled with 95% O_2/5% CO_2 , pH = 7.4) during the whole dissection. Slices were then transferred to artificial cerebrospinal fluid (ACSF: 119 mM NaCl, 5 mM KCl, 1.25 mM NaH_2PO_4, 1.5 mM $MgCl_2$, 2.5 mM $CaCl_2$, 26 mM $NaHCO_3$, and 10 mM dextrose, bubbled with 95% O_2/5% CO_2 , pH = 7.4) and incubated at 30° C for 30 min then room temperature (RT) for at least 30 min before recording.

For whole cell recording, acute 300 μm-thick hippocampal slices were similarly dissected except: 1) cold N-methyl-D-glucamine artificial cerebrospinal fluid (NMDG-ACSF) was used instead of dissection buffer for dissection. NMDG-ACSF contains (in mM): 93 NMDG, 2.5 KCl, 1.2 NaH_2PO_4·2 H_2O, 30 $NaHCO_3$, 20 HEPES, 5 Sodium ascorbate, 2 Thiourea, 3 Sodium pyruvate, 25 D-glucose, 0.5 $CaCl_2$, 10 $MgCl_2$, and bubbled with carbogen (95% O_2 and 5% CO_2). 2) Mice were transcardially perfused with ice-cold NMDAG-ACSF before sacrificed. 3) Slices were recovered for approximately 13 min in NMDG-ACSF at 30 ℃ before transferring to regular ACSF for at least 1 hr recover at RT.

4.2.2. fEPSP recording

fEPSP recording was done as previously describe (He et al., 2009a). Briefly, slices were transferred to submersion recording chambers perfused with ACSF (30 ± 0.5 ℃, 2 ml/min). Half maximal fEPSPs were evoked by stimulating the Schaffer collateral with 0.2 ms pulses delivered through customized double barrel glass electrodes (Sutter Instrument Co.) filled with ACSF. fEPSPs were recorded extracellularly in CA1 stratum radiatum filtered at 0–1000 Hz, digitized and stored at 5 K or 10 K sampling rate using customized program in Spike Hound (GK et al., 2009). Initial slope of AMPAR response or the amplitude of the pharmacologically isolated NMDAR response were analyzed using customized Matlab code.

4.2.2.1. Paired-pulse ratio (PPR). To measure PPR, 2 consecutive stimuli with inter-stimulus-intervals (ISIs) of 25, 50, 100, 250 and 500 ms were delivered to evoked paired responses. PPR was calculated as the slope of 2nd response over that of 1st response.

4.2.2.2. Input–output (IO) curve. To measure IO curve of AMPAR-mediated synaptic transmission, stimulation intensity was gradually increased with 4–5 repetitions of each intensity. Fiber volley (FV) amplitude was measured as input strength. IO curve of NMDARs was similarly measured by adding 10 μM CNQX to the ACSF to block AMPAR

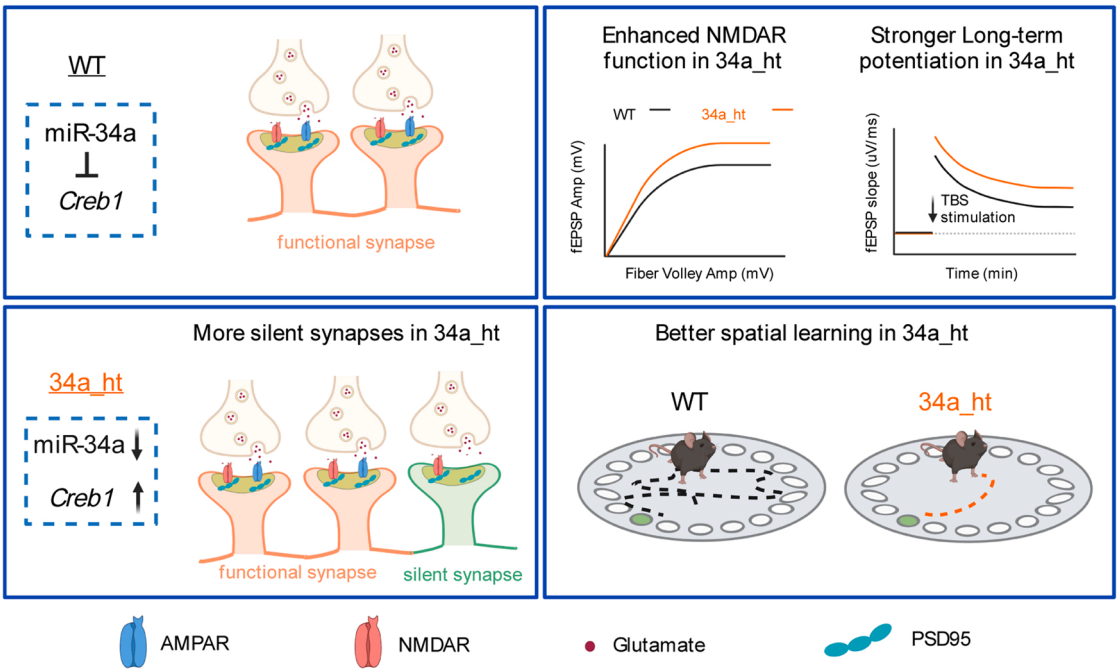

Fig. 7. Working model depicting the neuronal role of miR-34a in hippocampus of mature brain. In the hippocampus of adult 34a_ht mice, reduction in miR-34a promotes CREB1 expression, which then enhances levels of synaptic proteins including PSD95 and NMDARs. These results correlate with increased silent synapses in the 34a_ht mice. Thus, the Schaffer collateral synapses in the adult 34a_ht mice display stronger NMDAR-mediated synaptic transmission and larger TBS-induced LTP, which lead to better spatial learning and memory of the adult 34a_ht mice.

responses.

4.2.2.3. Long-term potentiation (LTP). Half maximal basal responses were evoked by delivering paired stimuli (ISI = 50 ms) at 0.033 Hz. After recording 30 min stable baseline, LTP was triggered by giving four trains of theta-burst stimulation (TBS) at 0.1 Hz. Each train consists of 10 bursts (four pulses at 100 Hz per burst) repeated at 5 Hz.

4.2.2.4. Long-term depression (LTD). 20 min stable baseline responses evoked by paired (ISI = 50 ms) stimulation delivered at 0.033 Hz was acquired. LTD was then induced by paired-pulse 1 Hz protocol (PP-1 Hz, paired pulses with 50 ms ISI delivered at 1 Hz for 15 min).

4.2.3. Whole-cell recordings of miniature excitatory postsynaptic currents (mEPSCs)

Whole-cell recordings of CA1 pyramidal neurons were carried out as previously described (He et al., 2015). Acute slices were transferred to a submerged recording chamber perfused with oxygenated ACSF with bath temperature maintained at 30 ± 0.5 °C. Cells were visualized under differential interference contrast using a 40x water immersion objective (Olympus XT640-W). Whole-cell current clamp recordings were obtained using an Axopatch 700B amplifier (Axon Instruments, Union City, CA). Data was filtered at 2 kHz and digitized at 10 kHz using Digidata 1550 A (Molecular Devices, CA, USA). Recording electrodes (3–5 MΩ) were filled with internal solutions containing: 8 mM KCl, 125 mM cesium gluconate, 10 mM HEPES, 1 mM EGTA, 4 mM MgATP, 0.5 mM NaGTP, and 5 mM QX-314, pH 7.2–7.3, 280–295 mOsm. Neurons were voltage clamped at − 70 mV during the recordings. Both input resistant Ri and access resistance Ra were monitored throughout the recording. Only cells with stable (less than 25% changes) Ri ≥ 100 MΩ and Ra ≤ 25 MΩ were used for analysis.

4.2.3.1. AMPAR-mEPSCs. AMPAR-mEPSCs were isolated by adding 1 μM TTX, 100 μM DL-APV and 10 μM gabazine to the perfusion ACSF. AMPAR-mEPSCs were analyzed using the MiniAnalysis program (Synaptosoft, Decatur, GA) as described previously (Michelle C.D. et al.,2020). Event detection threshold was set at 3 times over the RMS noise. At least 150 events with rise time < 3 msec were selected for each cell to calculate frequency and amplitude. And non-overlapping events were used to construct the average trace and estimate the decay time.

4.2.3.2. NMDAR-mEPSCs. 1 μM TTX, 10 μM CNQX and 10 μM gabazine was added to the Mg^{2+}-free ACSF to isolate NMDAR currents. In addition, 10 μM D-serine was added to facilitate NMDAR channel opening. For analysis, event detection threshold of NMDAR-mEPSCs was set at 2 times over the RMS noise and no rise time limitation. At least 100 events were selected for each cell to calculate frequency and amplitude.

4.2.4. Minimal stimulation assay

Minimal stimulation assay was performed as previously reported (Liao et al., 1995; Beroun et al., 2018; Graziane et al., 2016). Schaffer collateral synapses were stimulated at 0.2 Hz. CA1 pyramidal neurons were voltage clamped at − 60 mV and stimulation intensity was adjusted to evoked interleaved failures that could be visually distinguished. For each cell, 50–100 traces were recorded at − 60 mV and + 50 mV respectively. To estimate the percentage of silent synapses, failed versus successful trials of each recorded neuron were defined visually. Silent synapse percentage was calculated using the following equation: 1 - Ln (F_{-60})/ Ln (F_{+50}), in which F_{-60} was the failure rate at -60 mV and F_{+50} was the failure rate + 50 mV. Recording stability was chronically monitored by running seal test. Only cells began with access resistance Ra ≤ 20 MΩ and input resistance Rm ≥ 150 MΩ that remained stable (≤ 20% shift when holding at −60 mV), and reversed properly at positive holding voltage, were included for final analysis.

4.3. Lentivirus production and in vivo delivery

Lentiviruses were produced following published protocols (Ni et al., 2021). GFP were subcloned into pFHTrePW under control of a Tet Response Element (TRE 3 G). rtTA for tet-off system was expressed by pFHSynPW under the control of human synapsin I promoter.

Lentiviruses was delivered into hippocampus by stereotaxic

injection. Mice were head-fixed and maintained anesthetized by 1–2% isoflurane vapor. Ophthalmic ointment (Cisen, China) was applied to prevent eye dryness and mice were kept on a 37 ℃ heating pad. 500 nL Tet-off-GFP lentivirus was delivered at 50 nL/min via a microsyringe pump (Stoelting, USA) into dorsal CA1 Stratum Radiatum bilaterally (AP: −2.70 mm, ml: +/−2.25 mm, DV: −1.30 mm, relative to Bregma). After surgery animals returned to their home cages after fully awake. Virus was allowed to expressed for 12–14 days before imaging.

4.4. Immunostaining and confocal imaging

4.4.1. Brain sample preparation

Anesthetized mice were perfused transcardially with 10 ml 0.1 M cold sodium phosphate buffer (PBS) (4 ml/min) followed by 40 ml of 4% cold paraformaldehyde (PFA). Brains were removed and post-fixed in the same fixative overnight at 4 ℃. 100 μm thick transverse hippocampal slices (for spine imaging) or 50 μm thick coronal slices (for immunostaining) were sectioned using a vibratome (Lecia, VT1000s) in cold PBS and preserved in cryoprotectant solution (30% sucrose, 20% ethylene glycol and 50% 1 x PBS) at − 20 ℃ before used.

4.4.2. Immunostaining

50 μm thick fixed coronal brain slices containing target brain region were washed 3 times with 1x PBS. Slices were then blocked with PBS containing 5% goat serum and 0.1% Triton X-100 for 2 h at room temperature, and incubated with primary antibodies (P-Creb1, 1:1000, CST, #9198) overnight at 4 °C. Slices were washed three times in PBST before incubating with secondary antibodies for 2 h at room temperature and cover-slipped with mounting medium (SouthernBiotech, US, Prolong gold antifade reagent, Invitrogen).

4.4.3. Confocal Imaging

Spines were imaged using a scanning confocal microscope (Leica TCS SP8 X) using 488- nm Argon lasers and a 63x oil-immersion objective. Only secondary and tertiary basal dendrites of CA1 pyramidal neuron were imaged in a z-stack mode with the following resolution: x/y/z = 0.036/ 0.036/ 0.217 μm/pixel. Spine density was blindly analyzed by ImageJ (NIH) after z projection. 2–4 dendritic segments from individual CA1 pyramidal neurons, 2–3 neurons per mice, and 6 mice each from each genotype were imaged and analyzed for final comparison.

Fluorescence signal of P-Creb1 staining were acquired by using a spinning disk microscope (Andor) with a 20x air objective. P-Creb1 signal intensity of target brain region was analyzed using ImageJ after subtracting background signal.

4.5. Molecular biology

4.5.1. RNA extraction

Mice were anesthetized with isoflurane vapor and sacrificed. Hippocampi were quickly removed and transferred to an RNase-free tube and snap frozen in liquid nitrogen before used. Total RNA was extracted using TRIzol reagent (Invitrogen, Carlsbad, CA, USA) and purified by TURBO DNA-free™ Kit ((Invitrogen, Carlsbad, CA, USA). Final RNA concentration and RNA purity was determined using an ND-1000 spectrophotometer (Nanodrop Technologies Inc, Wilmington, DE, USA).

4.5.2. Quantitative RT-PCR

miR-34a/b/c were quantified by using TaqMan® Small RNA Assays (Applied Biosystems, Life Technologies) following the manufacturer's instructions. Specific assays against miR-34a/b/c were conducted (hsa-miR-34a, ID 000426; mmu-miR-34b-5p, ID 002617; hsa-miR-34c, ID 000428), snoRNA202 (ID 001232) as control.

4.5.3. Bulk RNA sequencing and data analysis

cDNA libraries were prepared using the VAHTS mRNA-seq V2 Library Prep Kit for Illumina. Libraries were sequenced by HiSeq platform (Illumina) by a 150-bp paired-end reads. Sequencing reads were mapped to the Ensembl annotation of the mouse C57BL/6 transcriptome. Read counts over transcripts were calculated using HTSeq followed by differential expression analysis using package DESeq (Anders and Huber. 2010). Genes were classified as differentially expressed based on the cutoff of FC> 1, P value < 0.05. GO term analysis was performed by Metascape (Zhou et al., 2019).

4.5.4. PSD preparation and western blotting

PSD preparation was carried out as previously describe (He et al., 2009b) and summarized in diagram in Sup Fig S3D. Solution used in this protocol were listed in Table S3.

The S1 (total protein fraction) and PSD (postsynapse-enriched fraction) were processed by SDS-PAGE and subjected to Western blotting. 10 μg S1 (total protein) or 1 ug PSD fractions were run on 8% SDS-polyacrylamide gels, which were then transferred onto polyvinylidene difluoride (PVDF) membranes (Bio-Rad, Hercules, CA, USA). The PVDF membranes were blocked with TBST containing 5% no-fat milk for 1 h at room temperature and then incubated with primary antibodies overnight at 4 °C. Subsequently, the membranes were washed before incubation with secondary antibodies for 1 h at room temperature. Blots were imaged and analyzed using chemiluminescence imaging system (Fusion, VILBER). Protein levels in S1 were normalized to α-tubulin, and those in PSD fractions were normalized to PSD95. All antibody used were listed in Table S2.

4.5.5. Firefly luciferase assay

The plasmids pcDNA3.1(+), pcDNA3.1(+)-Renilla and pcDNA3.1(+)-Firefly were generously gifted from Dr. Nan Liu's Laboratory (IRCBC). The 3′ UTR or Mut-3′UTR of Creb1 was subcloned into MCS downstream of the firefly luciferase gene using CMV as promoter. pri-miR-34a with extended 260 nucleotide in each direction was cloned into pcDNA3.1(+) vector. Primers used for all subcloning experiments were listed in Table S1.

Luciferase assay was performed using standard approach (Liu et al., 2012). Specifically, 3.5×10^4 HEK293T cells were plated and bathed in 200 μL DMEM medium supplemented with 10% inactivated fetal bovine serum (FBS) in each well of a 96 well plate. The next day, 200 ng of pcDNA3.1(+)-miR-34a, 50 ng of pcDNA3.1(+)-Renilla and 100 ng of pcDNA3.1(+)-Firefly-3′ UTR (WT or mutant reporters) were transfected by Lipofectamine 2000 (Invitrogen, Life). Luminescence assays were performed by Dual-Glo Luciferase Assay System (Promega) two days post transfection.

4.6. Behavior test

4.6.1. Novel location recognition task

The novel location recognition task (NOL) was performed as previously described (Bayraktar et al., 2021). Mice were handled 1 min daily for 3–5 days and habituated to the empty arena (40 cm × 40 cm wide by 60 cm tall) with clear visual cue 5 min each for another 4 days. Then mice were given 3 consecutive trainings with 10 min interval, 5 min each in the arena with two identical objects placed towards the same wall. Mice were allowed to rest in their home cages for 1 h before the test trial. In the test trial, one of the objects was removed to a novel location and mouse was allowed to explore for 5 min. All objects and the arena were cleaned with 75% ethanol between trials. The relative exploration time was recorded and discrimination index (DI) was calculated as [t-novel – t-familiar]/ [t-novel + t-familiar] × 100.

4.6.2. Barnes maze test

Barnes maze was performed as previously described (Pitts, 2018). The Barnes maze (OD = 90 cm) was placed in a brightly lit (~1000 lux) testing room with a camera mounted above. During habituation, mouse was first held in a holding tube opposing the escape hole for 15 s before

gently guided to the escape box and let stay for 2 min. Training sections were held at least 1 h post habituation and distinct visual cues were added to three walls of the room. Two continuous training sections were conducted for each mouse every day for 6 days. For each training, mouse was first placed in the center tube for 15 s. Then the tube was removed and a 90 dB white noise was turned on simultaneously. Mouse was given 180 s to find the escape box. It was guided to the box if it failed to find or enter the box within that time. The maze was cleaned used 75% ethanol and air dried between trials. One probe trial was held for each mouse on the 7th day with similar procedure except removing the escape box.

The latency, travel distance and average speed before entering the escape box were analyzed for each training section using Ethovision (Noldus, Wageningen, The Netherlands). And the number of incorrect holes checked prior to the correct locating (escape errors) was counted manually. To quantify the probe test, time spent in per quadrant and the number of pre-target hole checks were recorded.

4.6.3. Y maze

Spontaneous Y-maze was performed as previously described (Kraeuter et al., 2019; Suryavanshi et al., 2014). A custom-made Y-maze with three identical Plexiglas arms (30 × 6 × 12 cm, 120° apart) was placed at the center of a room under dim lighting conditions. Each mouse was placed at the end of one arm facing the center and allowed to explore the maze for 8 min. The sequence and total number of arms entered was recorded by Ethovision (Noldus, Wageningen, The Netherlands). Percent alternation was calculated as % Alternation = (Number of successful alternations) / (Total arm entries – 2) × 100.

4.7. Statistical analysis

Statistical analysis was performed by Prism V6.0 software (GraphPad Software, Inc.). Unpaired two-tailed Student's t-test was used to compare between two groups. One-way ANOVA followed by post hoc multiple comparison test (Bonferroni's or Tukey's) was used to compare data with more than 2 groups. Cumulative distributions were compared by Kolmogorov-Smirnov (KS) test. Error bars in all figures indicate standard error of mean (s.e.m). Only significant comparisons were labeled in the figures. The level of significance was set at $P < 0.05$. *$P < 0.05$; * *$P < 0.01$; * **$P < 0.001$; * ** *$P < 0.0001$.

Data Availability

Data will be made available upon request.

Acknowledgments

We thank Dr. Wenyuan Wang for kindly sharing the 34a_ht mice and Dr. Han Wang for helping with the firefly luciferase assay. We also thank the staff members of the animal facility at the National Facility for Protein Science in Shanghai (NFPS), Shanghai Advanced Research Institute, Chinese Academy of Sciences, China for excellent support. This work is supported by NSFC (Grant No. 31700917, 32070963, 32271004), Shanghai Science and Technology Development Funds (Grant No. 22ZR1475100), and Shanghai Municipal Science and Technology Major Project (Grant No. 2019SHZDZX02) to K.-W.H.

CRediT authorship contributions statement

Conceptualization, K.-W.H.; Investigation, X.M., J.-Y. W., F.-J.Z.; Data Analysis, X.M.; Writing, X.M. and K.-W.H.; Funding Acquisition, K.-W.H; Supervision, K.-W.H.

Competing Interest Statement

The authors report no competing interests.

Appendix A. Supporting information

Supplementary data associated with this article can be found in the online version at doi:10.1016/j.pneurobio.2023.102404.

References

Abe, M., Bonini, N.M., 2013. MicroRNAs and neurodegeneration: role and impact. Trends Cell Biol. 23, 30–36.
Agostini, M., et al., 2011. microRNA-34a regulates neurite outgrowth, spinal morphology, and function. Proc. Natl. Acad. Sci. USA 108, 21099–21104.
Aguado, F., et al., 2009. The CREB/CREM transcription factors negatively regulate early synaptogenesis and spontaneous network activity. J. Neurosci. 29, 328–333.
Aranha, M.M., Santos, D.M., Sola, S., Steer, C.J., Rodrigues, C.M., 2011. miR-34a regulates mouse neural stem cell differentiation. PLoS One 6, e21396.
Ashby, M.C., Isaac, J.T., 2011. Maturation of a recurrent excitatory neocortical circuit by experience-dependent unsilencing of newly formed dendritic spines. Neuron 70, 510–521.
Bartel, D.P., 2009. MicroRNAs: target recognition and regulatory functions. Cell 136, 215–233.
Bayraktar, G., Hojgaard, K., Nijssen, L., Takeuchi, T., 2021. A within-subject experimental design using an object location task in rats. J. Vis. Exp.
Beroun, A., et al., 2018. Generation of silent synapses in dentate gyrus correlates with development of alcohol addiction. Neuropsychopharmacology 43, 1989–1999.
Bie, B., 2018. Amyloid fibrils induce dysfunction of hippocampal glutamatergic silent synapses. Hippocampus 28, 549–556.
Birdsong, D., 2018. Plasticity, variability and age in second language acquisition and bilingualism. Front Psychol. 9, 81.
Bommer, G.T., et al., 2007. p53-mediated activation of miRNA34 candidate tumor-suppressor genes. Curr. Biol. 17, 1298–1307.
Brown, T.E., et al., 2011. A silent synapse-based mechanism for cocaine-induced locomotor sensitization. J. Neurosci. 31, 8163–8174.
Busetto, G., Higley, M.J., Sabatini, B.L., 2008. Developmental presence and disappearance of postsynaptically silent synapses on dendritic spines of rat layer 2/3 pyramidal neurons. J. Physiol. 586, 1519–1527.
Carroll, R.C., Zukin, R.S., 2002. NMDA-receptor trafficking and targeting: implications for synaptic transmission and plasticity. Trends Neurosci. 25, 571–577.
Chang, S.J., et al., 2011. MicroRNA-34a modulates genes involved in cellular motility and oxidative phosphorylation in neural precursors derived from human umbilical cord mesenchymal stem cells. BMC Med Genom. 4, 65.
Chang, T.C., et al., 2007. Transactivation of miR-34a by p53 broadly influences gene expression and promotes apoptosis. Mol. Cell 26, 745–752.
Chen, P., Chen, F., Lei, J., Li, Q., Zhou, B., 2019. Activation of the miR-34a-Mediated SIRT1/mTOR signaling pathway by urolithin A attenuates d-galactose-induced brain aging in mice. Neurotherapeutics 16, 1269–1282.
Cogswell, J.P., et al., 2008. Identification of miRNA changes in Alzheimer's disease brain and CSF yields putative biomarkers and insights into disease pathways. J. Alzheimers Dis. 14, 27–41.
Collingridge, G.L., Peineau, S., Howland, J.G., Wang, Y.T., 2010. Long-term depression in the CNS. Nat. Rev. Neurosci. 11, 459–473.
Dean, P., Porrill, J., Ekerot, C.F., Jorntell, H., 2010. The cerebellar microcircuit as an adaptive filter: experimental and computational evidence. Nat. Rev. Neurosci. 11, 30–43.
Gebert, L.F.R., MacRae, I.J., 2019. Regulation of microRNA function in animals. Nat. Rev. Mol. Cell Biol. 20, 21–37.
GK, L., BR, J., RH, B., BR, L., RR, H., 2009. g-PRIME: a free, windows based data acquisition and event analysis software package for physiology in classrooms and research lab. J. Under Neurosci. Ed. 8, 5.
Gonzalez, G.A., Montminy, M.R., 1989. Cyclic AMP stimulates somatostatin gene transcription by phosphorylation of CREB at serine 133. Cell 59, 675–680.
Goto, A., et al., 2021. Stepwise synaptic plasticity events drive the early phase of memory consolidation. Science 374, 857–863.
Graziane, N.M., et al., 2016. Opposing mechanisms mediate morphine- and cocaine-induced generation of silent synapses. Nat. Neurosci. 19, 915–925.
Hanse, E., Seth, H., Riebe, I., 2013. AMPA-silent synapses in brain development and pathology. Nat. Rev. Neurosci. 14, 839–850.
He, K., et al., 2009b. Stabilization of Ca2+-permeable AMPA receptors at perisynaptic sites by GluR1-S845 phosphorylation. Proc. Natl. Acad. Sci. USA 106, 20033–20038.
He, K., et al., 2015. Distinct eligibility traces for LTP and LTD in cortical synapses. Neuron 88, 528–538.
He, K.W., et al., 2009a. Stabilization of Ca2+-permeable AMPA receptors at perisynaptic sites by GluR1-S845 phosphorylation. Proc. Natl. Acad. Sci. USA 106, 20033–20038.
Hu, Y.R., Xing, S.L., Chen, C., Shen, D.Z., Chen, J.L., 2019. Tiaoxin recipe, a Chinese herbal formula, inhibits microRNA-34a expression in the APPswe/PS1DeltaE9 mouse model of Alzheimer's disease. J. Integr. Med. 17, 404–409.
Huang, Q., et al., 2017. The miR-34a/Bcl-2 pathway contributes to auditory cortex neuron apoptosis in age-related hearing loss. Audio Neurootol. 22, 96–103.
Huang, X., et al., 2015. Progressive maturation of silent synapses governs the duration of a critical period. Proc. Natl. Acad. Sci. USA 112, E3131–3140.
Isaac, J.T.R., Nicoll, R.A., Malenka, R.C., 1995. Evidence for silent synapses: Implications for the expression of LTP. Neuron 15, 427–434.
Jauhari, A., Singh, T., Singh, P., Parmar, D., Yadav, S., 2018. Regulation of miR-34 family in neuronal development. Mol. Neurobiol. 55, 936–945.

Jian, C., et al., 2017. miR-34a knockout attenuates cognitive deficits in APP/PS1 mice through inhibition of the amyloidogenic processing of APP. Life Sci. 182, 104–111.
Kerchner, G.A., Nicoll, R.A., 2008. Silent synapses and the emergence of a postsynaptic mechanism for LTP. Nat. Rev. Neurosci. 9, 813–825.
Kohr, G., 2006. NMDA receptor function: subunit composition versus spatial distribution. Cell Tissue Res 326, 439–446.
Korn, H., Faber, D.S., 1991. Quantal analysis and synaptic efficacy in the CNS. Trends Neurosci. 14, 439–445.
Kosik, K.S., 2006. The neuronal microRNA system. Nat. Rev. Neurosci. 7, 911–920.
Kou, X., et al., 2017. Swimming attenuates d-galactose-induced brain aging via suppressing miR-34a-mediated autophagy impairment and abnormal mitochondrial dynamics. J. Appl. Physiol. 1985 122, 1462–1469.
Kou, X., Liu, X., Chen, X., Jie, L., Ning, C., 2016. Ampelopsin attenuates brain aging of D-gal-induced rats through miR-34a-mediated SIRT1/mTOR signal pathway. Oncotarget 7.
Koya, E., et al., 2012. Silent synapses in selectively activated nucleus accumbens neurons following cocaine sensitization. Nat. Neurosci. 15, 1556–1562.
Kraeuter, A.K., Guest, P.C., Sarnyai, Z., 2019. The Y-maze for assessment of spatial working and reference memory in mice. Methods Mol. Biol. 1916, 105–111.
Kreitzer, A.C., Malenka, R.C., 2008. Striatal plasticity and basal ganglia circuit function. Neuron 60, 543–554.
Lau, C.G., Zukin, R.S., 2007. NMDA receptor trafficking in synaptic plasticity and neuropsychiatric disorders. Nat. Rev. Neurosci. 8, 413–426.
Lee, B.R., et al., 2013. Maturation of silent synapses in amygdala-accumbens projection contributes to incubation of cocaine craving. Nat. Neurosci. 16, 1644–1651.
Lee, H.K., Min, S.S., Gallagher, M., Kirkwood, A., 2005. NMDA receptor-independent long-term depression correlates with successful aging in rats. Nat. Neurosci. 8, 1657–1659.
Lee, S.H., et al., 2007. Nuclear translocation of CAM-associated protein activates transcription for long-term facilitation in Aplysia. Cell 129, 801–812.
Liao, D., Hessler, N.A., Malinow, R., 1995. Activation of postsynaptically silent synapses during pairing-induced LTP in CA1 region of hippocampal slice. Nature 375, 400–404.
Lisman, J., Cooper, K., Sehgal, M., Silva, A.J., 2018. Memory formation depends on both synapse-specific modifications of synaptic strength and cell-specific increases in excitability. Nat. Neurosci. 21, 309–314.
Liu, N., et al., 2012. The microRNA miR-34 modulates ageing and neurodegeneration in Drosophila. Nature 482, 519–523.
Lonze, B.E., Ginty, D.D., 2002. Function and regulation of CREB family transcription factors in the nervous system. Neuron 35, 605–623.
Marie, H., Morishita, W., Yu, X., Calakos, N., Malenka, R.C., 2005. Generation of silent synapses by acute in vivo expression of CaMKIV and CREB. Neuron 45, 741–752.
Martin, S.J., Grimwood, P.D., Morris, R.G., 2000. Synaptic plasticity and memory: an evaluation of the hypothesis. Annu Rev. Neurosci. 23, 649–711.
Mollinari, C., et al., 2015. miR-34a regulates cell proliferation, morphology and function of newborn neurons resulting in improved behavioural outcomes. Cell Death Dis. 6, e1622.
Morgado, A.L., et al., 2015. MicroRNA-34a modulates neural stem cell differentiation by regulating expression of synaptic and autophagic proteins. Mol. Neurobiol. 51, 1168–1183.
Nakayama, K., Kiyosue, K., Taguchi, T., 2005. Diminished neuronal activity increases neuron-neuron connectivity underlying silent synapse formation and the rapid conversion of silent to functional synapses. J. Neurosci. 25, 4040–4051.
Naqvi, S., Martin, K.J., Arthur, J.S., 2014. CREB phosphorylation at Ser133 regulates transcription via distinct mechanisms downstream of cAMP and MAPK signalling. Biochem J. 458, 469–479.
Neves, G., Cooke, S.F., Bliss, T.V., 2008. Synaptic plasticity, memory and the hippocampus: a neural network approach to causality. Nat. Rev. Neurosci. 9, 65–75.
Ni, J., et al., 2021. Loss of TDP-43 function underlies hippocampal and cortical synaptic deficits in TDP-43 proteinopathies. Mol. Psychiatry.
Nowakowski, T.J., et al., 2018. Regulation of cell-type-specific transcriptomes by microRNA networks during human brain development. Nat. Neurosci. 21, 1784–1792.
Paoletti, P., Bellone, C., Zhou, Q., 2013. NMDA receptor subunit diversity: impact on receptor properties, synaptic plasticity and disease. Nat. Rev. Neurosci. 14, 383–400.
Paraskevopoulou, M.D., et al., 2013. DIANA-microT web server v5.0: service integration into miRNA functional analysis workflows. Nucleic Acids Res. 41, W169–W173.
Pitts, M.W., 2018. Barnes maze procedure for spatial learning and memory in mice. Bio Protoc. 8.
Reczko, M., Maragkakis, M., Alexiou, P., Grosse, I., Hatzigeorgiou, A.G., 2012. Functional microRNA targets in protein coding sequences. Bioinformatics 28, 771–776.
Redman, S., 1990. Quantal analysis of synaptic potentials in neurons of the central nervous system. Physiol. Rev. 70, 165–198.
Riebe, I., Gustafsson, B., Hanse, E., 2009. Silent synapses onto interneurons in the rat CA1 stratum radiatum. Eur. J. Neurosci. 29, 1870–1882.
Sametsky, E.A., Disterhoft, J.F., Geinisman, Y., Nicholson, D.A., 2010. Synaptic strength and postsynaptically silent synapses through advanced aging in rat hippocampal CA1 pyramidal neurons. Neurobiol. Aging 31, 813–825.
Sarkar, S., et al., 2016. Expression of microRNA-34a in Alzheimer's disease brain targets genes linked to synaptic plasticity, energy metabolism, and resting state network activity. Brain Res. 1646, 139–151.
Sarkar, S., et al., 2019. Over-expression of miR-34a induces rapid cognitive impairment and Alzheimer's disease-like pathology. Brain Res 1721, 146327.
Schratt, G., 2009. microRNAs at the synapse. Nat. Rev. Neurosci. 10, 842–849.
Shukla, A., et al., 2017. Calcium-permeable AMPA receptors and silent synapses in cocaine-conditioned place preference. EMBO J. 36, 458–474.
Sun, H., et al., 2018. Early seizures prematurely unsilence auditory synapses to disrupt thalamocortical critical period plasticity. Cell Rep. 23, 2533–2540.
Suryavanshi, P.S., Ugale, R.R., Yilmazer-Hanke, D., Stairs, D.J., Dravid, S.M., 2014. GluN2C/GluN2D subunit-selective NMDA receptor potentiator CIQ reverses MK-801-induced impairment in prepulse inhibition and working memory in Y-maze test in mice. Br. J. Pharmacol. 171, 799–809.
Telese, F., et al., 2015. LRP8-reelin-regulated neuronal enhancer signature underlying learning and memory formation. Neuron 86, 696–710.
Vincent-Lamarre, P., Lynn, M., Beique, J.C., 2018. The eloquent silent synapse. Trends Neurosci. 41, 557–559.
Wang, Y., Liu, Y.Z., Wang, L., Tang, W., Wang, Z., 2019. Silent synapse unsilencing in hippocampal CA1 neurons for associative fear memory storage. Cereb. Cortex 29, 4067–4076.
Wang, Y.Q., et al., 2021. Neuropathic pain generates silent synapses in thalamic projection to anterior cingulate cortex. Pain 162, 1322–1333.
Watson, D.J., et al., 2016. LTP enhances synaptogenesis in the developing hippocampus. Hippocampus 26, 560–576.
Wright, W.J., et al., 2020. Silent synapses dictate cocaine memory destabilization and reconsolidation. Nat. Neurosci. 23, 32–46.
Xu, W., Lowel, S., Schluter, O.M., 2020. Silent synapse-based mechanisms of critical period plasticity. Front Cell Neurosci. 14, 213.
Xu, Y., Chen, P., Wang, X., Yao, J., Zhuang, S., 2018. miR-34a deficiency in APP/PS1 mice promotes cognitive function by increasing synaptic plasticity via AMPA and NMDA receptors. Neurosci. Lett. 670, 94–104.
Yusifov, R., Tippmann, A., Staiger, J.F., Schluter, O.M., Lowel, S., 2021. Spine dynamics of PSD-95-deficient neurons in the visual cortex link silent synapses to structural cortical plasticity. Proc. Natl. Acad. Sci. USA 118.
Zhou, Y., et al., 2019. Metascape provides a biologist-oriented resource for the analysis of systems-level datasets. Nat. Commun. 10, 1523.